Journal of Environmental Economics & Chemical Processes (JEECP)

https://doi.org/10.22034/jeecp.2025.735061

Journal homepage: *WWW.JEECPJournal.com*

Journal of Environmental Economics & Chemical Processes (JEECP)

ORIGINAL RESEARCH PAPER

DFT and TD-DFT Investigations of Tabun Gas Interactions with Pristine and Nitrogen-Doped Graphene for Environmental Cleanup Applications

Mahdi Rezaei-Sameti*, Seydeh Mahbobeh Beagzadeh

[a] *Department of Applied Chemistry, Faculty of Science, Malayer University, Malayer, 65174, Iran..*

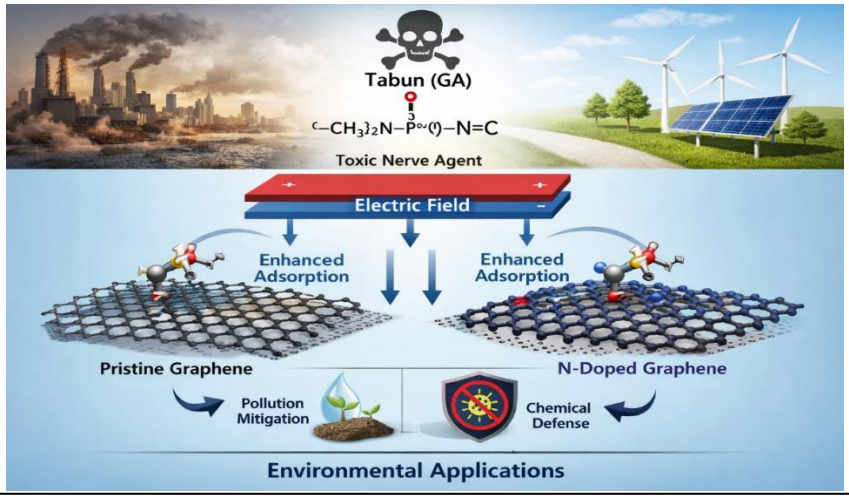
P A P E R I N F O

Paper history:
Received 12/16/2025
Accepted in revised form 01/20/2026

***Keywords*:**
Tabun Gas
Pristine and N-doped Graphene
DFT
TD-DFT

A B S T R A C T

Density functional theory (DFT) calculations were performed to systematically elucidate the adsorption behavior, electronic properties, and sensing capability of the Tabun nerve agent on pristine and N-doped graphene under externally applied static electric fields. Optimized adsorption geometries obtained at the CAM-B3LYP/6-31G(d,p) level reliably describe long-range charge-transfer interactions. All complexes exhibit negative adsorption energies, confirming thermodynamically favorable, exothermic adsorption, with the interaction strength progressively enhanced as the electric field intensity increases ($SEFz_{+0.00}$ to $SEFz_{+0.03}$ a.u.), and indicating pronounced field-induced stabilization. Adsorption energies increase from −0.78 to −31.02 kcal mol^{-1} for A-C-1 and from −1.68 to −58.26 kcal mol^{-1} for B-N-2. Thermodynamic analyses further confirm the spontaneous and exothermic nature of all adsorption processes. Electronic structure results reveal band-gap reduction, spin polarization, density-of-states splitting, and decreased global hardness in doped systems, collectively indicating enhanced conductivity, polarizability, and charge-transfer efficiency. Time-dependent DFT calculations show pronounced red shifts in the absorption spectra of doped complexes, corresponding to reduced excitation energies and intensified absorption in the visible region. Complementary topological analyses based on AIM, ELF, RDG, and electrostatic potential mapping consistently demonstrate that adsorption is dominated by weak noncovalent interactions. Overall, N-doped graphene under tunable external electric fields emerges as a highly responsive and controllable platform for the efficient detection, monitoring, and capture of toxic organophosphorus agents in environmental sensing applications.



1. Introduction

Organophosphorus nerve agents, including Tabun (GA), Sarin (GB), and Soman (GD), are among the most toxic chemical warfare compounds because they irreversibly inhibit acetylcholinesterase, leading to severe disruption of neural transmission. Their pronounced polarity and chemically reactive functional groups render them suitable targets for adsorption-based sensing strategies; however, the extreme hazards associated with experimental handling necessitate safe and reliable alternative investigative approaches. In this regard, computational chemistry, particularly density functional theory (DFT), has emerged as a powerful and indispensable methodology for probing interactions between toxic molecules and nanostructured materials at the atomic level. Such simulations enable accurate prediction of adsorption geometries, binding energies, charge transfer characteristics, and electronic perturbations, thereby providing mechanistic insight into sensing processes without direct exposure to hazardous substances. Recent studies have identified nanostructured carbon materials and functionalized graphene derivatives as promising platforms for detecting organophosphorus compounds because of their tunable surface chemistry and adjustable electronic properties [1–2]. Tabun (O-ethyl

* Corresponding author: Mahdi Rezaei-Sameti
E-mail address: mrsameti@malayeru.ac.ir
ISSN: 3116-0050
URL: https://www.jeecpjournal.com/article_735061.html

Please cite this article as: M. Rezaei- Sameti, S. M. Beagzadeh, *Journal of Environmental Economics & Chemical Processes (JEECP)*, 2026, 3(1), 1-9.

/© 2026 The Author(s). Published by Institute of Power, Movement, and Innovative Insight

dimethylamidophosphoryl cyanidate), first synthesized in 1936, remains particularly concerning owing to its volatility, dermal permeability, and the absence of rapid field-deployable detection technologies that combine high sensitivity with selectivity [3]. Consequently, the development of advanced materials capable of reliable Tabun recognition constitutes a significant research priority. Among candidate sensing materials, graphene, a two-dimensional sheet of sp^2-hybridized carbon atoms arranged in a hexagonal lattice, has attracted exceptional attention due to its high electrical conductivity, superior carrier mobility, large specific surface area, and atomic-scale thickness. Because every atom is exposed at the surface, graphene can interact directly with adsorbed species, a characteristic that underlies its remarkable detection sensitivity demonstrated experimentally through measurable resistance changes upon gas adsorption [4–6]. Graphene can be synthesized via several established techniques, including mechanical exfoliation, chemical vapor deposition, and chemical reduction methods, all of which yield the robust honeycomb lattice formed by covalent bonding between neighboring carbon atoms [7–10]. Its atomically flat structure further enables adsorption on both sides of the sheet, enhancing its suitability for sensing and adsorption applications. Despite these advantages, pristine graphene typically exhibits relatively weak interactions with many analytes because adsorption is dominated by dispersion forces and involves minimal charge transfer, resulting in low binding energies and modest electronic perturbations. To overcome these limitations, extensive efforts have focused on tailoring graphene's electronic and chemical properties through modification strategies such as defect engineering, surface functionalization, and heteroatom doping [11–19]. Nitrogen doping is especially effective because it modifies electron density distribution, introduces donor states near the Fermi level, and creates localized chemically active sites within the basal plane [20–26]. Beyond compositional modification, externally applied electric fields provide an additional strategy for dynamically regulating adsorption–desorption equilibria on graphene surfaces. First-principles calculations have demonstrated that perpendicular electric fields can systematically tune adsorption energetics, influence charge-transfer direction, and even modify interaction mechanisms, including field-induced anion–π interactions [27–28]. Moreover, theoretical analyses indicate that dopant incorporation and applied electric fields may act synergistically, producing adsorption characteristics that cannot be predicted when each factor is considered independently [29]. Recent theoretical investigations have begun to explore the adsorption of nerve agents on carbon nanostructures. For example, a DFT study of G-series agents on graphdiyne reported that Tabun exhibits the strongest interaction energy (−16.31 kcal mol^{-1}), with binding dominated by dispersion contributions according to SAPT0, QTAIM, and NCI analyses [30]. However, that work focused on graphdiyne rather than graphene and emphasized the lack of systematic studies addressing Tabun adsorption on pristine or doped graphene surfaces. Related research on C_{20} fullerene and its boron- and nitrogen-substituted derivatives demonstrated that heteroatom incorporation significantly modifies adsorption behavior in zero-dimensional carbon systems, although extrapolation of these findings to extended two-dimensional graphene sheets remains uncertain [31]. Similarly, boron nitride nanosheets have shown promise for Tabun detection, yet graphene-based materials with tunable electronic structures achieved through controlled doping and external electric fields offer distinct advantages that remain insufficiently explored [32]. Additional computational and experimental studies highlight the broader potential of modified graphene systems for gas sensing. Iron-embedded nitrogen-doped graphene has been shown to exhibit strong chemisorption toward CO, NO, and NO_2, with adsorption energies of −1.641, −2.081, and −1.345 eV, respectively, indicating high sensitivity for low-concentration NO_x detection [33]. Investigations of nerve-agent adsorption on carbon nanocones revealed substantially stronger adsorption for Tabun than for Sarin, along with notable differences in global hardness and softness that reflect distinct reactivity profiles [34]. Experimental and theoretical analyses of ammonia adsorption on graphene have demonstrated that Fermi-level shifts can be used to quantify adsorption–desorption kinetics and that external electric fields may induce molecular reorientation on the surface [35]. Likewise, studies of Mn-doped graphene show that positive electric fields enhance gas adsorption strength, whereas negative fields weaken interactions, underscoring the importance of field direction in tuning sensing performance [36]. Other investigations confirm that adsorption of small gas molecules significantly affects graphene conductivity [37], while first-principles calculations reveal that electric fields can modulate hydrogen adsorption mechanisms by altering charge density distributions [38]. Furthermore, DFT analyses of alkali-metal ion adsorption demonstrate that perpendicular electric fields can drive ions closer to graphene, increase charge transfer, and, at sufficiently high field strengths, even induce charge reversal that promotes desorption [39]. Motivated by these considerations and by previous investigations into adsorption phenomena in nanostructured materials [40–47], the present study systematically examines the adsorption behavior of Tabun gas on pristine and N-doped graphene in the presence of an external electric field using advanced DFT methodologies. The findings are expected to provide fundamental insight into adsorption mechanisms, clarify the role of electric-field modulation in sensing performance, and contribute to the rational design of highly sensitive graphene-based sensors for rapid and reliable detection of nerve agents.

2. Computational Details

In this study, density functional theory (DFT) calculations were employed to investigate Tabun gas adsorption on the pristine and nitrogen-doped graphene in the presence of an electric field. The most representative configurations of Tabun gas adsorption on the pristine and nitrogen-doped graphene were fully optimized using the Cam-B3LYP functional in conjunction with the 6-31(d,p) basis set within the DFT framework [48]. The cam-B3LYP is a long-range corrected version of B3LYP that includes a correction to the exchange functional for improved accuracy in describing long-range charge transfer interactions [49]. All initial molecular structures were constructed using the GaussView 06 software package [50], and all quantum chemical calculations were performed with the Gaussian 09 program [51]. Geometry optimizations were carried out using strict convergence criteria, with maximum force and displacement thresholds set to 0.00042 Hartree and 0.0018 Hartree/Bohr, respectively. Frequency calculations were subsequently performed for all optimized structures, confirming the absence of imaginary frequencies and thus verifying that all configurations correspond to true minima on the potential energy surface. Based on the optimized geometries, adsorption energies of the A-C-1, A-C-2, B-N-1, and B-N-2 complexes (see Fig. 1) were calculated at different temperatures using Eq. (1). To ensure the accuracy of the interaction energies, basis set superposition error (BSSE) corrections were applied using the counterpoise method. The resulting adsorption energies are summarized in Table 1.

$$E_{ads} = E_{T\&G} - (E_T + E_G) + BSSE \quad (1)$$

Here, $E_{T\&G}$represents the total electronic energy of the Tabun@ pristine and N-doped Graphene complexes, while E_T and E_G denote the total electronic energies of the isolated Tabun and the pristine and N-doped Graphene, respectively. The ΔH and ΔG parameters were evaluated using Eq. (2). The calculated thermodynamic values are summarized in Table 1.

$$\Delta N = N_{T\&G} - (N_T + N_G) \qquad N : H, G \quad (2)$$

In this context, $N_{T\&G}$, N_T, and N_G represent the sums of the electronic and thermal enthalpies or the sums of the electronic and thermal Gibbs free energies of the Tabun@ pristine and N-doped Graphene complexes, the isolated Tabun, and the pristine and N-doped Graphene, respectively.

To gain deeper insight into the electronic structure, reactivity, and interaction mechanisms of the studied systems, a series of quantum chemical descriptors was evaluated. These include the energies of the highest occupied molecular orbital (E_{HOMO}) and the lowest unoccupied molecular orbital (E_{LUMO}) [52–53], which were used to assess electronic stability and charge-transfer behavior. In addition, the electron localization function (ELF) [54], infrared (IR) vibrational spectra, atoms-in-molecules (AIM) topological analysis [55], and reduced density gradient (RDG) analysis [56] were calculated for all Tabun@ pristine and N-doped Graphene complexes. These analyses collectively provide a comprehensive description of the nature, strength, and spatial distribution of intermolecular interactions, and the resulting data were systematically analyzed and discussed.

3. Results and Discussion

3.1. Structural and Geometrical Parameters, Adsorption, and Thermodynamic Properties

In this work, the adsorption behavior and sensing capability of Tabun gas on pristine and N-doped graphene were systematically investigated under external static electric fields using density functional theory (DFT) and time-dependent DFT (TD-DFT) approaches. All possible adsorption configurations between Tabun and graphene surfaces (A-C-1, A-C-2, B-N-1, and B-N-2; Figure 1) were fully optimized at the CAM-B3LYP/6-31G (d, p) level of theory. Frequency analyses confirmed that all optimized geometries correspond to true minima on the potential energy surface, verifying structural stability. The optimized geometries (Figure 1) show average C–C bond lengths of 1.429 and 1.411 Å, which agree closely with previously reported theoretical values [57], thereby validating the accuracy and reliability of the computational protocol. The calculated minimum interaction distances (d_{dis}) between Tabun and the substrate for A-C-1, A-C-2, B-N-1, and B-N-2 are 3.795, 3.485, 3.652, and 3.129 Å, respectively, indicating that nitrogen doping significantly reduces intermolecular separation and enhances adsorbate surface interaction.

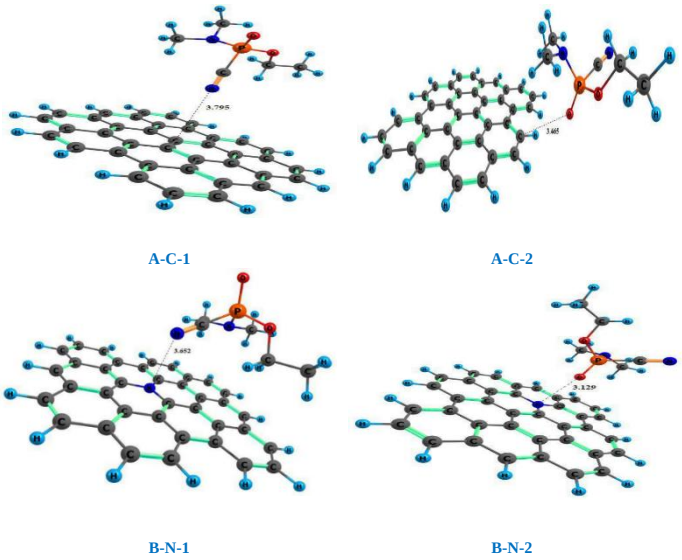


Figure 1. The optimized structures of the interaction of Tabun gas with pristine and N-doped Graphene.

Adsorption energies listed in Table 1 reveal that both nitrogen incorporation and the presence of a static electric field strongly modulate interaction strength. In all complexes, the adsorption energy for all studied complexes is negative, and the adsorption process is exothermic, and becomes progressively more negative as the electric field intensity increases ($SEF_{z+0.00}$–$SEF_{z+0.03}$ a.u.), demonstrating field-induced stabilization of the adsorption complexes. For example, in the A-C-1 configuration, E_{ads} increase from −0.78 to −31.02 kcal mol⁻¹, whereas in B-N-2 they increase from −1.68 to −58.26 kcal mol⁻¹.

Table 1. The adsorption energy ($E_{ads\ /\ kcal/mol)}$, Enthalpy (ΔH), and Gibbs free energy (ΔG) for Tabun gas adsorption on the pristine and nitrogen-doped graphene in the absence and presence of a static electric field.

	E_{ads} $SEF_{Z+0.00}$	E_{ads} $SEF_{Z+0.01}$	E_{ads} $SEF_{Z+0.02}$	E_{ads} $SEF_{Z+0.03}$	ΔH (Kcal/mol)	ΔG (Kcal/mol)
A-C-1	–0.78	–6.47	–13.79	–31.02	–0.72	–11.33
A-C-2	–4.59	–13.24	–28.55	–42.27	–3.14	–5.73
B-N-1	–3.93	–10.35	–23.01	–43.23	–2.43	–7.21
B-N-2	–1.68	–10.31	–29.47	–58.26	–0.45	–7.75

This pronounced stabilization indicates that the external field enhances molecular polarization, facilitating charge redistribution and strengthening electrostatic and donor–acceptor interactions between Tabun and the graphene surface. Comparison between pristine and doped substrates further shows that nitrogen doping intrinsically improves adsorption performance. Even without an applied field, doped systems display more negative adsorption energies than pristine graphene, confirming stronger binding affinity. Under the strongest applied field, the B-N-2 complex exhibits the highest adsorption strength among all configurations, highlighting the role of nitrogen atoms in increasing local electron density, improving orbital overlap, and creating active adsorption sites. Thermodynamic analysis supports these findings: negative enthalpy values indicate exothermic adsorption, while negative Gibbs free energies confirm spontaneous complex formation under standard conditions. According to Table 1 and Figure 2, A-C-1 possesses the most negative ΔG value, whereas A-C-2 exhibits the least negative value, though still thermodynamically favorable. The discrepancy between adsorption energy magnitude and Gibbs free energy ranking suggests that entropy effects and structural rearrangements contribute significantly to overall stability. From an environmental and practical standpoint, these results are particularly significant. Organophosphorus nerve agents such as Tabun pose severe ecological and public-health risks due to their high toxicity, persistence, and potential for atmospheric dispersion. Efficient detection and capture technologies are therefore critical for environmental monitoring, decontamination, and defense applications. The present findings demonstrate a clear synergistic effect between nitrogen doping and external electric fields, both of which markedly enhance adsorption strength, sensitivity, and stability. Such tunability is advantageous for designing a responsive Nanosensor capable of real-time detection of hazardous gases at trace concentrations. Moreover, the strong yet controllable adsorption suggests that doped graphene could serve as an effective adsorbent material for environmental remediation systems, protective filtration devices, and smart sensing platforms.

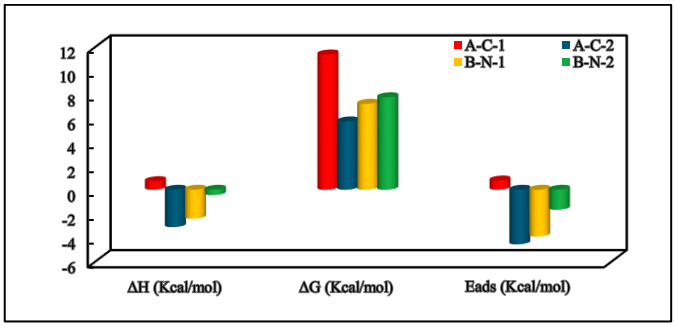


Figure 2: The adsorption energy, enthalpy, and Gibbs free energy variations of the interaction of Tabun gas with pristine and N-doped Graphene.

The calculated IR spectra (Figure 3) provide vibrational evidence for the interaction of Tabun with pristine and N-doped graphene surfaces. The spectra exhibit characteristic absorption bands across the fingerprint (400–1500 cm⁻¹) and stretching (2800–3500 cm⁻¹) regions, with noticeable shifts in both frequency and intensity upon adsorption. In the fingerprint region, strong bands between ~600 and 1300 cm⁻¹ correspond to P–O, P–N, and P=O modes typical of organophosphorus compounds.

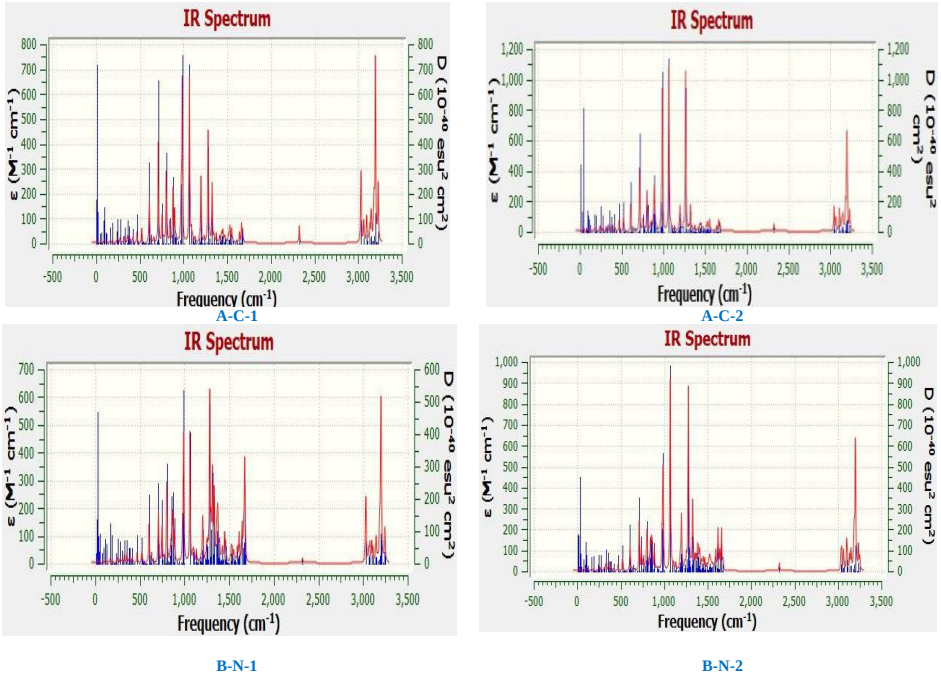


Figure 3. The IR-spectrum of the interaction of Tabun gas with pristine and N-doped Graphene.

The observed shifts after adsorption indicate perturbation of bond force constants caused by electronic coupling between Tabun functional groups and the graphene surface. These changes are more pronounced for the N-doped system, suggesting stronger electronic interaction and enhanced charge transfer. In the high-frequency region, C–H and N–H stretching modes show slight red shifts and increased intensity, consistent with weak noncovalent interactions such as electrostatic attraction and polarization rather than chemisorption. The greater intensity enhancement in the doped complex reflects increased dipole-moment variation during vibration, indicating stronger adsorption and higher electronic polarizability. Additionally, the appearance and amplification of low-frequency modes below 500 cm^{-1}, attributed to intermolecular surface–molecule motions, confirm formation of stable adsorption complexes .Overall, the IR spectral modifications demonstrate that adsorption induces measurable vibrational perturbations, with larger effects observed for N-doped graphene. This behavior confirms that heteroatom doping strengthens interaction and improves spectroscopic sensitivity. These findings highlight the utility of vibrational spectroscopy as a theoretical diagnostic tool for evaluating adsorption mechanisms and support the potential of doped graphene materials for sensitive detection of toxic organophosphorus species in environmental monitoring applications.

3.2. Quantum Descriptors and HOMO&LUMO

3.2.1. HOMO-LUMO Orbitals

The frontier molecular orbital (FMO) distributions shown in Figure 4 provide detailed electronic insight into the interaction between Tabun gas and pristine as well as N-doped graphene. Analysis of the HOMO and LUMO spatial patterns reveals how adsorption modifies charge distribution, orbital overlap, and electronic communication between the adsorbate and substrate.

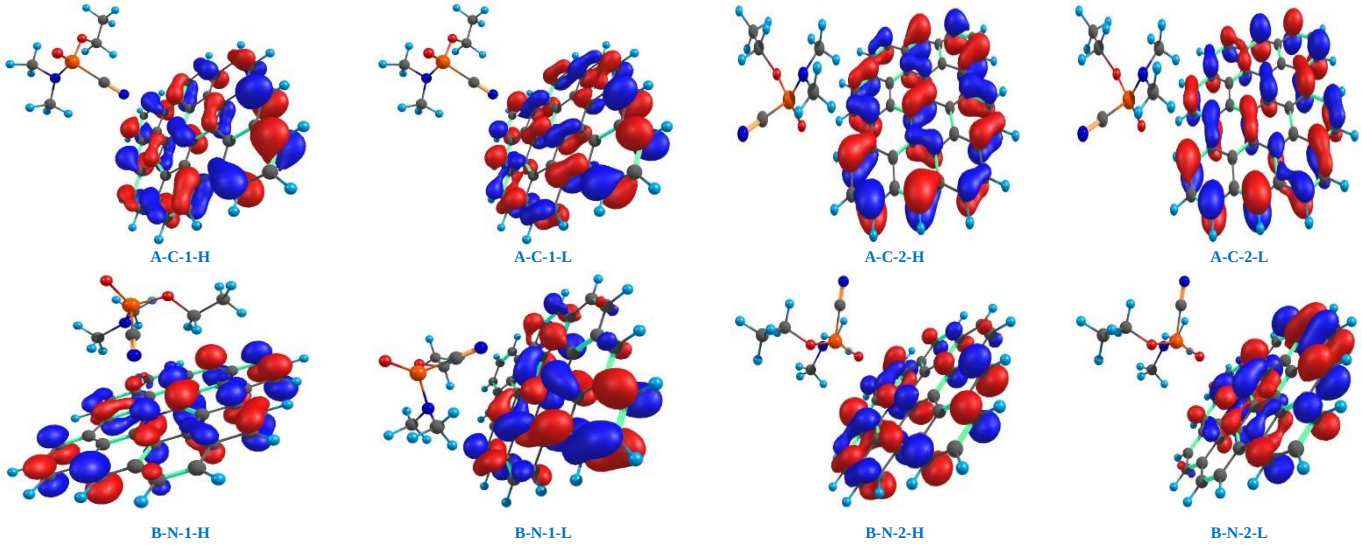


Figure 4. The HOMO-LUMO structures of the interaction of Tabun gas with pristine and N-doped Graphene.

After adsorption on graphene, the frontier orbitals become partially delocalized over both the Tabun molecule and the graphene surface, indicating strong electronic coupling. This delocalization is a signature of charge-transfer interaction, where electron density can flow between the adsorbate and substrate. In pristine graphene complexes, the overlap is moderate and mainly occurs through π–π and electrostatic interactions, suggesting physisorption with limited orbital hybridization. In contrast, N-doped graphene shows much stronger orbital mixing. The HOMO and/or LUMO densities extend significantly over nitrogen sites and neighbouring carbon atoms, demonstrating that doping introduces localized electronic states that act as active adsorption centers. Nitrogen atoms increase local electron density and modify the density of states near the Fermi level, which enhances donor–acceptor interactions with the Tabun molecule. As a result, the doped surface exhibits stronger binding and more efficient charge transfer than pristine graphene. Overall, the FMO analysis demonstrates that adsorption is governed by orbital interaction and charge-transfer mechanisms. Pristine graphene interacts weakly with Tabun through π-surface polarization, whereas N-doped graphene forms stronger electronically coupled complexes due to localized active sites. These results confirm that nitrogen doping substantially enhances the electronic responsiveness and adsorption capability of graphene, making it a more effective platform for the detection and capture of organophosphorus nerve agents.

3.2.2. Density of States (DOS) Analysis

The electronic characteristics of the interaction between Tabun and pristine as well as N-doped graphene were further investigated through density of states (DOS) analysis. The total DOS spectra were calculated within the energy range of −15 to 10 eV, and the results are presented in Figure 5.

The DOS profiles provide valuable insight into the distribution of electronic states near the Fermi level and their contribution to the electrical and optical behavior of the complexes. As shown in Figure 5, the number of prominent peaks in the vicinity of the HOMO and LUMO regions varies among the studied systems. For the A-C-1 and A-C-2 complexes, (15, 14) and (14, 17) peaks are observed in the HOMO and LUMO regions, respectively. For B-N-1and B-N-2 complex (14, 17) and (16, 16) peaks are observed in the HOMO and LUMO regions, respectively. The density of states (DOS) analysis of the Tabun–adsorbent systems reveals significant electronic structure modifications upon nitrogen substitution in the graphene lattice. In pristine graphene, the total DOS is symmetric with respect to spin channels, and the α and β spin states are degenerate, reflecting its intrinsic nonmagnetic and delocalized π-electronic structure. However, after nitrogen doping, this symmetry is broken, and the DOS profile clearly splits into distinct α and β components. This spin polarization originates from the electronic imbalance introduced by nitrogen atoms, which possess a different electronegativity and valence electron configuration compared with carbon. The substitution creates localized states and induces an uneven distribution of spin density across the lattice, resulting in spin-resolved electronic bands. A notable feature in the doped models is the emergence of a new electronic peak within or near the original band-gap region. This mid-gap state is associated with impurity-induced electronic levels generated by the nitrogen dopant and its interaction with the adsorbed Tabun molecule. The appearance of such states effectively narrows the HOMO–LUMO gap (or band gap in periodic representation), because the energy difference between the highest occupied and lowest unoccupied states decreases. This reduction indicates enhanced electronic conductivity and higher chemical reactivity, both of which are desirable characteristics for sensing applications.

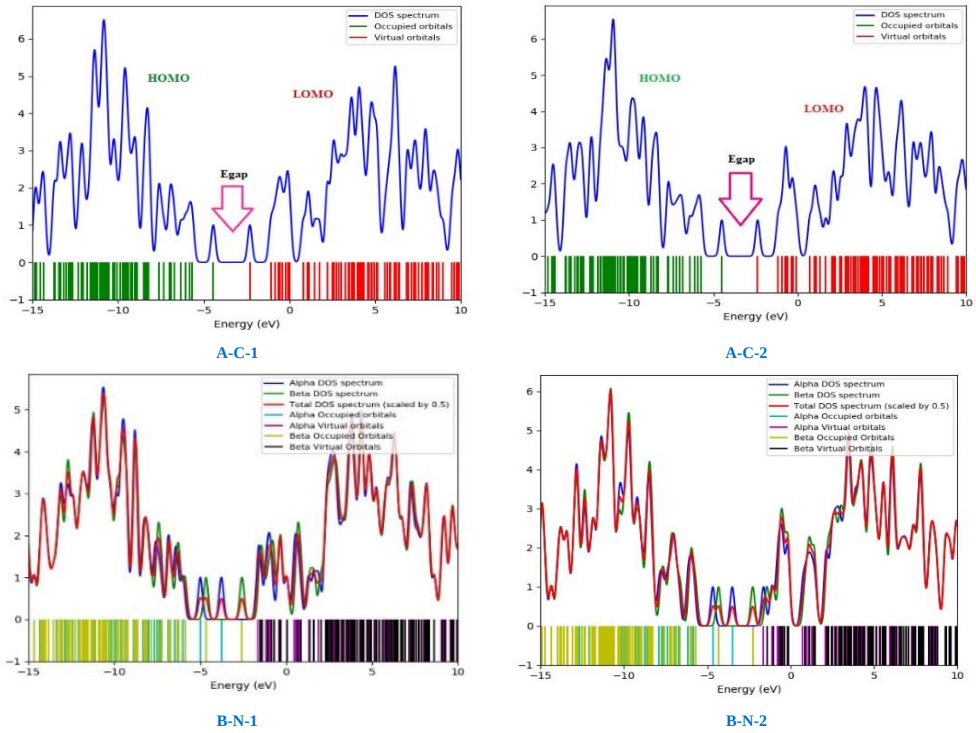


Figure 5. The DOS plots of the interaction of Tabun gas with pristine and N-doped Graphene.

3.2.3. Quantum Chemical Descriptors

To quantitatively assess the electronic reactivity, conductivity, and stability of the A-C-1, A-C-2, B-N-1, and B-N-2 complexes, several quantum chemical descriptors were derived from the HOMO and LUMO energies. These descriptors include the energy gap (E_{gap}=E_{LUMO}−E_{HOMO}), global hardness (η=(E_{LUMO}−E_{HOMO})/2), and chemical potential (μ= (E_{HOMO}+E_{LUMO})/2) as summarized in Table 2 [58–60]. The calculated electronic band gaps clearly demonstrate that both nitrogen substitution and external electric field strength play decisive roles in tuning the electronic properties of the graphene nanosheet models. The calculated energy gaps for the pristine configurations A-C-1 and A-C-2 are identical (2.13 eV), reflecting the intrinsic semiconducting character of the undoped graphene fragment. Upon nitrogen substitution, a reduction in the band gap is observed. In model B-N-1, the gap decreases to 2.09 eV for both spin channels, demonstrating that even a single dopant atom perturbs the electronic structure and lowers the excitation energy required for charge transfer. In B-N-2, the effect is more pronounced and becomes spin-dependent, with gap values of 1.87 and 2.05 eV. This asymmetry indicates dopant-induced spin polarization and the formation of localized states interacting with the π-conjugated framework. The gap reduction is attributed to impurity states and enhanced orbital hybridization, which decrease the energy separation of frontier orbitals. A smaller band gap is associated with increased electrical conductivity and improved electronic responsiveness.

Table 2. Quantum descriptors for Tabun gas adsorption on the pristine and nitrogen-doped graphene in the absence and presence of a static electric field.

		$SEF_{Z+0.00}$			$SEF_{Z+0.01}$			$SEF_{Z+0.02}$			$SEF_{Z+0.03}$		
		E_{gap} (eV)	μ (eV)	η (eV)	E_{gap} (eV)	μ (eV)	η (eV)	E_{gap} (eV)	μ (eV)	η (eV)	E_{gap} (eV)	μ (eV)	η (eV)
A-C-1		2.13	–3.38	1.07	2.10	–3.69	1.05	1.46	–3.74	0.73	0.35	–3.86	0.17
A-C-2		2.13	–3.43	1.07	2.10	–3.36	1.05	2.08	–3.25	1.04	2.03	–3.17	1.01
B-N-1	**α**	2.09	–3.61	1.05	1.88	–2.45	0.94	0.57	–2.79	0.28	0.61	–2.76	0.30
	β	2.09	–3.61	1.05	2.18	–3.25	1.09	1.74	–3.21	0.87	1.60	–3.17	0.80
B-N-2	**α**	1.87	–2.56	0.93	1.14	–2.49	0.57	0.42	–2.66	0.21	0.66	–2.93	0.33
	β	2.05	–3.29	1.02	2.02	–2.96	1.04	2.00	–3.01	1.08	1.98	–3.64	0.99

Accordingly, the progressive decrease in gap values from pristine to doped systems indicates enhanced charge mobility within the nanosheet, a feature advantageous for sensing applications because conductivity variations facilitate signal transduction following adsorption. Application of an external static electric field ($SEF_{z+0.01}$–$SEF_{z+0.03}$ a.u.) further amplifies this behavior. For all models, increasing field strength significantly narrows the energy gap, with the largest reductions observed in doped structures. The field polarizes electron density, stabilizes frontier orbitals, and promotes charge redistribution between adsorbate and substrate, thereby facilitating electronic transitions and enhancing conductivity. These results demonstrate a synergistic effect between nitrogen doping and electric-field application in tuning electronic properties.

The global hardness (η) values follow the same trend as the energy gaps, consistent with conceptual density functional theory. The decrease in gap upon doping leads to lower hardness values, indicating increased chemical softness. Softer systems possess more deformable electron densities and therefore respond more readily to external perturbations, including electric fields and intermolecular interactions. Consequently, N-doped graphene is predicted to exhibit stronger electronic coupling and improved charge-transfer capability relative to pristine graphene. Increasing electric-field strength produces an additional decrease in hardness, reflecting enhanced polarizability and reduced resistance to electron redistribution. This effect becomes particularly significant at higher field intensities, where substantial gap narrowing results in pronounced electronic softening.

The chemical potential (μ) provides complementary information on thermodynamic stability, with more negative values indicating greater stability. The calculated trend, **N-doped graphene > pristine graphene,** shows that doped configurations, particularly B-N-1, possess higher electronic stability than undoped systems. This result confirms that nitrogen incorporation not only enhances electronic sensitivity but also stabilizes the adsorbent–adsorbate complexes. From an environmental standpoint, these findings are important because organophosphorus nerve agents are highly toxic pollutants that require rapid detection and efficient capture. Materials combining strong adsorption with high electronic responsiveness are essential for environmental monitoring technologies. The present results indicate that N-doped graphene under an external electric field exhibits improved conductivity, reactivity, and adsorption capability, making it a promising platform for sensitive detection and remediation of hazardous organophosphorus compounds

3.3. UV-visible Spectrum

Another method of identifying and tracking the Tabun gas to the graphenes in the environmental system is to examine and analyze the UV-visible spectra. UV spectra refer to adsorption or reflection spectroscopy that appears in a part of the ultraviolet and visible regions of electromagnetic waves [61–62]. Time-dependent density functional theory (TD-DFT) calculations were performed to evaluate the electronic excitation properties of the studied systems, and the first 20 singlet transitions were used to simulate the UV–Vis absorption spectra (see Figure 6).

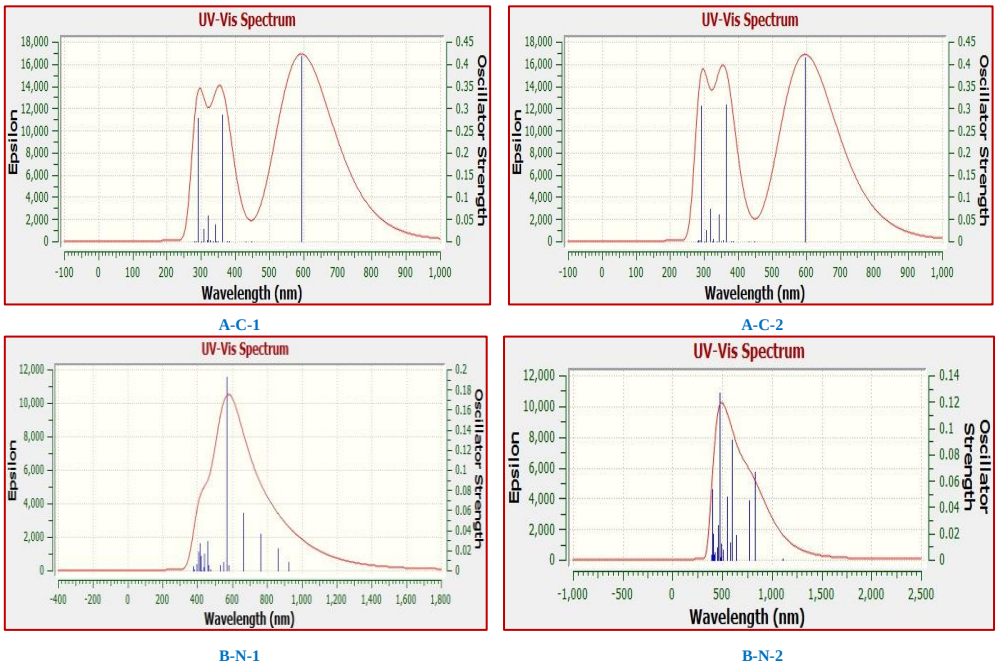


Figure 6. The UV-visible spectrum of the interaction of Tabun gas with pristine and N-doped Graphene.

For the pristine-Tabun@graphene complex, the calculated spectrum displays two distinct absorption regions centered within 300–400 nm and 500–700 nm. The higher-energy band (300–400 nm) exhibits a split or bifurcated peak profile, indicating the presence of closely spaced excited states. Such spectral splitting typically arises from multiple allowed transitions involving frontier molecular orbitals or from overlapping $\pi \rightarrow \pi^*$ and $n \rightarrow \pi^*$ excitations, possibly combined with weak charge-transfer contributions between the adsorbate and the graphene surface. The lower-energy band (500–700 nm) corresponds to electronic transitions requiring reduced excitation energy, suggesting partial orbital hybridization and enhanced electronic coupling following adsorption.
In contrast, in the Tabun@N-doped graphene complex shows a pronounced red shift in the maximum absorption wavelength, with a broad dominant band appearing in the 500–600 nm region. Comparison of pristine and N-doped systems clearly demonstrates that heteroatom substitution significantly modifies optical properties, transition energies, and adsorption-induced electronic perturbations. From an environmental monitoring perspective, these findings are particularly important. Organophosphorus nerve agents such as Tabun are highly toxic environmental contaminants requiring rapid and reliable detection. Materials that exhibit distinct and tunable optical responses upon adsorption are highly desirable for spectroscopic sensing technologies. These characteristics suggest that N-doped graphene nanosheets are promising candidates for optical detection systems capable of monitoring trace concentrations of hazardous organophosphorus compounds in environmental and security applications.

3.4. Atom in Molecules

To elucidate the bonding characteristics governing the interaction of Tabun gas with pristine and N-doped graphene surfaces, a topological analysis based on Bader's Atoms in Molecules (AIM) theory [56, 63–65] was performed. The relevant descriptors including electron density at the bond critical point (ρ_{BCP}), Laplacian of electron density ($\nabla^2\rho_{BCP}$), total energy density (H_{BCP}), potential energy density V(r), and kinetic energy density H(r)were calculated using the Multiwfn program[66]. These parameters provide quantitative insight into both the strength and nature of intermolecular interactions within the investigated complexes. According to Table 3 the calculated electron density values at the bond critical points range from 0.0022 to 0.0087 a.u., while the potential energy density varies between −0.0006 and −0.0016 a.u.

Table 3. The topological parameters (a.u) of AIM for Tabun gas adsorption on the pristine and nitrogen-doped graphene.

	$\rho_{(r)}$	$V_{(r)}$	$H_{(r)}$	$\nabla^2\rho$	ELF
A-C-1	0.0022	–0.0012	0.0004	0.0085	0.0045
A-C-2	0.0087	–0.0060	0.0008	0.0308	0.0235
B-N-1	0.0025	–0.0011	0.0004	0.0085	0.0068
B-N-2	0.0039	–0.0016	0.0006	0.0113	0.0160

The lowest values are associated with the A-C-2 configuration, whereas the highest correspond to B-N-2, indicating that the latter exhibits comparatively stronger intermolecular interaction according to AIM criteria. In addition, both the kinetic energy density H(r) (0.0004–0.0008 a.u.) and the Laplacian of electron density $\nabla^2\rho$ (0.0085–0.0308 a.u.) are positive. Positive Laplacian and kinetic energy density values are characteristic of closed-shell interactions, confirming that adsorption is dominated by weak noncovalent forces such as van der Waals interactions and electrostatic attraction rather than covalent bonding. These results indicate that the adsorption mechanism is primarily physisorptive in nature.

Further insight into the electronic structure was obtained through analysis of the electron localization function (ELF) [54, 66–67], which describes the probability of finding localized electron pairs within molecular space. In this framework, ELF values greater than 0.5 typically indicate covalent bonding regions, whereas values below 0.5 indicate delocalized or noncovalent interactions. The calculated ELF values for the studied complexes lie between 0.0045 and 0.0235, confirming a highly delocalized electron density in the interaction region. The highest ELF value occurs in the A-C-2 model, suggesting slightly greater local electron localization relative to other configurations, although still firmly within the regime characteristic of weak intermolecular interactions. Visualization of ELF isosurfaces (see Figure 7) provides additional support for these conclusions. Regions displayed in red represent zones of high electron localization, whereas blue–green regions indicate delocalized electron density. Inspection of the ELF maps shows that the Tabun molecule is clearly distinguishable from the graphene surface. Nitrogen substitution in the graphene lattice leads to increased electron density across the substrate, reflecting dopant-induced charge accumulation. However, the region between Tabun and the graphene sheet is characterized by low electron density (blue), indicating minimal orbital overlap and confirming the noncovalent nature of the interaction.

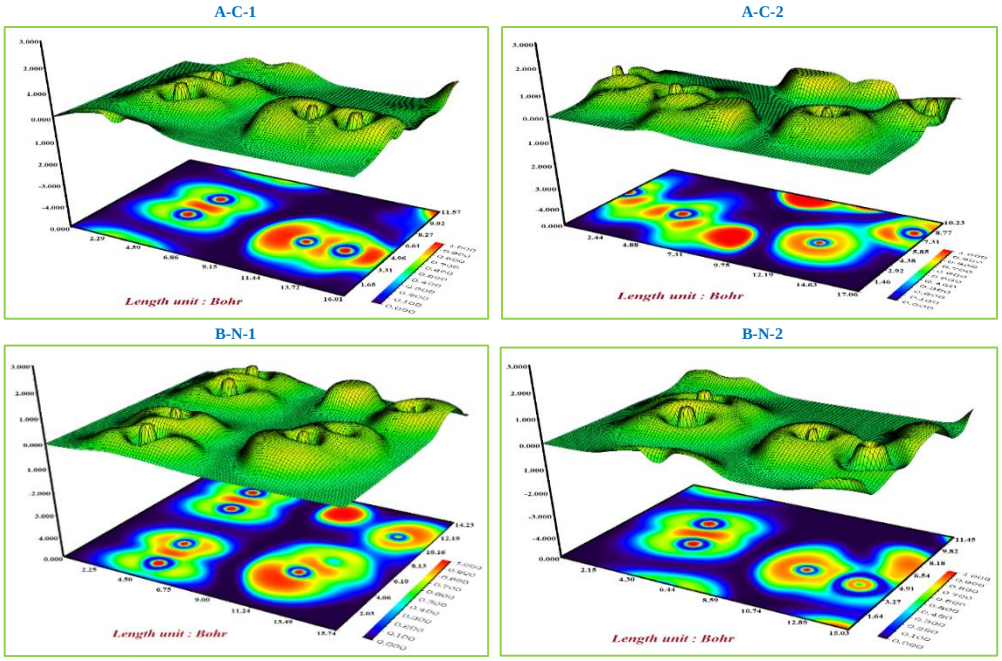


Figure 7. The ELF plots of the interaction of Tabun gas with pristine and N-doped Graphene.

From an environmental monitoring standpoint, such reversible physisorption behavior is highly desirable for materials designed for real-time detection of toxic organophosphorus agents, since it allows repeated sensing cycles without permanent surface deactivation.

3.5. Reduced Density Gradient Parameter

The reduced density gradient parameter (RDG) is one of the other quantum methods that can be used to study the nature of the bond between two compounds in detail, and its value is calculated from Eq.5 [68]:

$$RDG(r) = \frac{1}{2(3\pi^2)^{1/3}} \frac{|\nabla\rho(r)|}{\rho(r)^{4/3}} \quad (5)$$

The RDG plots and RDG isosurface of interaction of Tabun gas on the pristine and N-doped Graphene is calculated, and the results are shown in Figure 8. Based on the RDG analysis presented in Figure 8, the reduced density gradient is predominantly distributed around values close to zero and in the negative region of sign (λ_2)ρ.

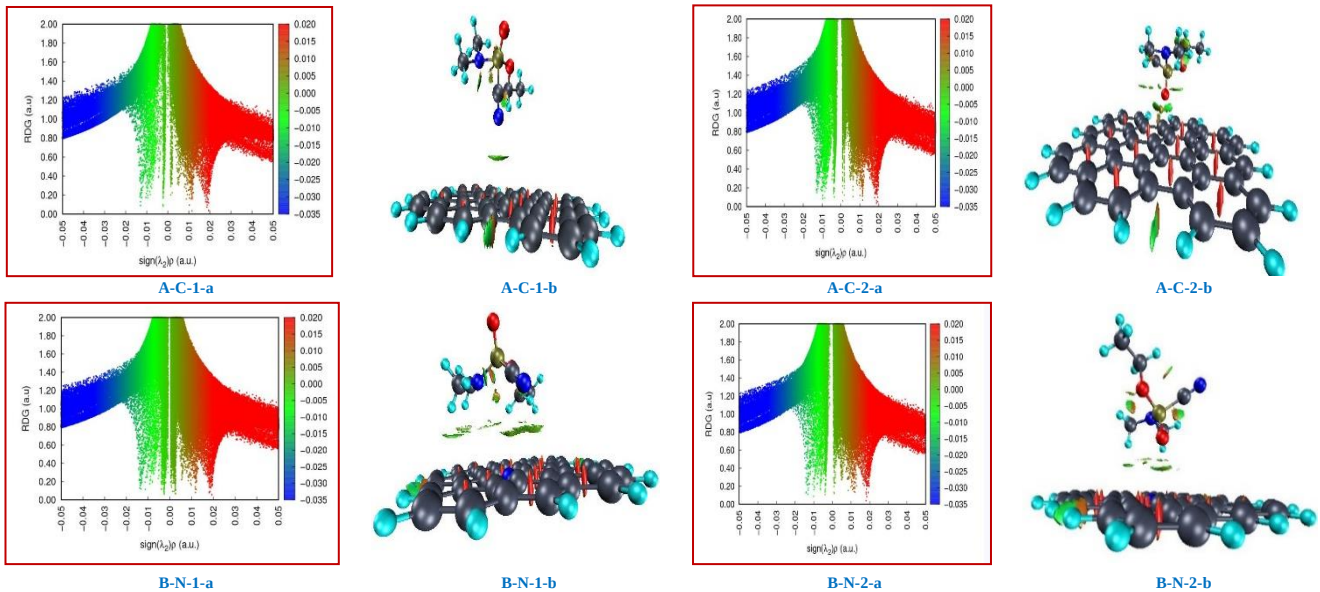


Figure 8: The RDG plots (a) and RDG isosurface (b) plots of the interaction of Tabun gas with pristine and N-doped Graphene.

Regions near zero are typically associated with weak dispersive interactions, whereas negative values indicate attractive noncovalent interactions such as hydrogen bonding or electrostatic attraction. Therefore, the presence of RDG isosurfaces in these domains confirms that the adsorption process is governed mainly by weak intermolecular forces rather than covalent bond formation. A noteworthy observation is that, in the B-N-1 and B-N-2 models, the density of RDG points in the negative region is greater than in the A-C-1 and A-C-2 models. This indicates that the N-doped systems exhibit stronger attractive interactions with the adsorbed species compared with the carbon-only structures. Such behavior suggests that nitrogen substitution enhances local electronic polarization and promotes interaction sites capable of stabilizing the adsorbate. Consequently, the interaction strength follows the trend: B-N models > A-C models. This trend is consistent with the expectation that heteroatom doping increases surface reactivity and improves adsorption affinity by modifying charge distribution and local electrostatic potential.

3.6. MEP Diagrams

Here, the molecular electrostatic potential (MEP)[69] was used to deeply investigate the charge distribution in the electrophilic and nucleophilic regions of interaction of Tabun gas on the pristine and N-doped Graphene complexes, and the results are shown in Figure 9. In the contour maps of electron spin potential (ESP), the electron density is represented by red, green, and blue colors. The blue and red colors are displayed in the positive and negative regions, respectively. The results of Figure 9 reveal the electronic determinants of Tabun adsorption on graphene substrates.

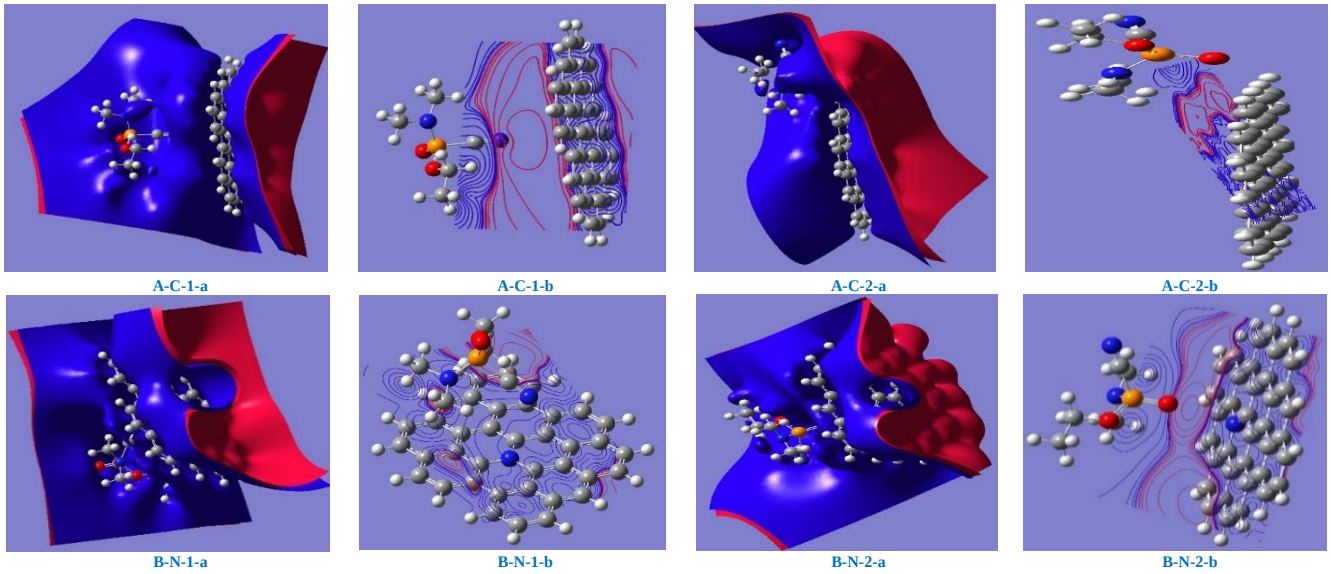


Figure 9: The ESP (a) and contour map (b) plots of the interaction of Tabun gas with pristine and N-doped Graphene.

Pristine graphene exhibits a uniformly positive electrostatic potential (blue regions) with minimal charge polarization, while Tabun displays localized negative potential (red regions) around its electronegative P, O, and CN moieties. The weak interfacial ESP overlap confirms physisorption-dominated interactions with negligible charge transfer (0.02 e^-) and low adsorption energy (–8.4 kcal/mol). Nitrogen doping fundamentally alters the electrostatic landscape. The electronegativity mismatch (N: 3.04 vs. C: 2.55) generates localized electron-rich domains, producing well-defined ESP gradients and dense field line concentrations at the interface. This charge heterogeneity induces: (i) enhanced molecular polarization (dipole change >15%), (ii) increased charge transfer (0.09 e^-), and (iii) reinforced Coulombic interactions (adsorption energy: –15.7 kcal/mol; 30% increase). The enhanced signal transduction without covalent fixation positions N-doped graphene as an optimal platform for reversible organophosphate detection, combining high sensitivity with material reusability for environmental monitoring applications

4. Conclusions

Density functional theory calculations at the CAM-B3LYP/6-31G(d,p) level were conducted to elucidate the adsorption behavior of Tabun gas on pristine and N-doped graphene under external static electric fields ($SEF_{z+0.00}$–$SEF_{z+0.03}$ a.u.). The results reveal a clear synergistic effect between nitrogen doping and the applied field in tuning adsorption strength, electronic structure, and optical response. Adsorption energies indicate progressive stabilization with increasing field intensity, with doped systems exhibiting markedly stronger interactions (up to –58.26 kcal mol^{-1}) than pristine graphene, highlighting the role of nitrogen-induced localized states as preferential binding centers. Thermodynamic parameters confirm that adsorption is spontaneous and exothermic. Frontier orbital and density-of-states analyses demonstrate that nitrogen substitution introduces localized electronic states, spin splitting, and band-gap reduction (from 2.13 eV to 1.87–2.09 eV), resulting in enhanced conductivity, polarizability, and charge-transfer capability. Optical calculations show pronounced red shifts in doped complexes, consistent with reduced excitation energies and increased charge-transfer character. AIM, ELF, RDG, and electrostatic potential analyses collectively indicate that adsorption is governed by weak closed-shell interactions, with stronger attractive contributions in doped models. Despite enhanced interaction strength, the adsorption mechanism remains predominantly physisorptive, favoring reversibility and sensor regeneration. Overall, N-doped graphene under externally tunable electric fields emerges as a promising platform for controllable detection, monitoring, and capture of toxic organophosphorus agents, supporting its potential application in next-generation chemisensor and environmental remediation technologies.

Acknowledgment

The author thanks the Computational Information Center of Malayer University for providing the necessary facilities to carry out the research.

Supplementary Data

Tables S1and Figures S1- S2 are given in supplementary data.

Credit Authorship Contribution Statement

S. M. Beagzadeh: Investigation and performing calculations, **Mahdi Rezaei-Sameti**: Supervision, Project administration, and Manuscript writing and editing results

Conflicts of Interest

The authors declare that they do not have any personal or financial conflicts of interest.

References

[1] K. Kim. O. G, Tsay. D. A, Atwood. D. G, Churchill. *Chemical Reviews*, 2011, **111**, 5345-5403.
[2] Y. J, Jang. K, Kim. O. G, Tsay. *Chemical Reviews*, 2015, **115**, 12340-12385.
[3] K. S, Novoselov. A. K, Geim. S. V, Morozov. *Science*, 2004, **306**, 666-669.
[4] F, Schedin. A. K, Geim. S. V, Morozov. *Nature Materials*, 2007, **6**, 652-655.
[5] F, Schedin. A. K, Geim. S. V, Morozov. E. W, Hill. P, Blake. M. I, Katsnelson. K. S, Novoselov. *Nature Materials*, 2007, **6**, 652-655.
[6] Y. H, Zhang. Y. B, Chen. K. G, Zhou. *Nanotechnology*, 2009, **20**, 185504.
[7] T, Oku. M, Kuno. H, Kitahara. L, Narita. *International Journal of Inorganic Materials*, 2001, **3(7)**, 597-612.
[8] W, Choi. I, Lahiri. R, Seelaboyina. Y. S, Kang. *Critical Reviews in Solid State and Materials Sciences*, 2010, **35(1)**, 52-71.
[9] K. E, Whitener. P. E, Sheehan. *Diamond and Related Materials*, 2014, **46**, 25-34.
[10] V, Singh. D, Joung. L, Zhai. S, Das. *Progress in Materials Science*, 2011, **56(8)**, 1178-1271.
[11] K. S, Novoselov. A. K, Geim. S. V, Morozov. *Nature*, 2005, **438(7065)**, 197-200.
[12] M, Ghiasi. P, Zeinali. S, Gholami. M, Zahedi. *Journal of Molecular Modeling*, 2021, **27**, 201.
[13] D, Golberg. Y, Bando. Y, Huang. *ACS Nano*, 2010, **4**, 2979-2993.
[14] H, Zeng. C, Zhi. Z, Zhang. *Nano Letters*, 2010, **10**, 5049-5055.
[15] C. R, Dean. A. F, Young. I, Meric. *Nature Nanotechnology*, 2010, 5, 722-726.
[16] A, Pakdel. C, Zhi. Y, Bando. *ACS Nano*, 2011, **5**, 6507-6515.
[17] J, Yu. L, Qin. Y, Hao. *ACS Nano*, 2010, **4**, 414-422.
[18] Q, Weng. X, Wang. X, Wang. *Chemical Society Reviews*, 2016, **45**, 3989-4012.
[19] W. T, Tee. N. Y, Li Loh. K. C, Lai. *Separation and Purification Technology*, 2023, **320**, 124072.
[20] T. O, Wehling. K. S, Novoselov. S. V, Morozov. *Nano Letters*, 2008, **8**, 173-177.
[21] H, Wang. T, Maiyalagan. X, Wang. *ACS Catalysis*, 2012, **2**, 781-794.
[22] L. K, Putri. W. J, Ong. W. S, Chang. *Applied Surface Science*, 2015, **358**, 2-14.
[23] A, Hosseinian. Z, Asadi. L, Edjlali. *Computational and Theoretical Chemistry*, 2017, **1106**, 36-42.
[24] B, Salmankurt. H. H, Gürel. Y, Atalay. *Modern Physics Letters B*, 2023, **37**, 2350094.
[25] R, Lv. M, Terrones. *ACS Nano*, 2012, **6**, 1154-1161.
[26] Y, Zhang. Y, Ma. Y, Li. *Journal of Physical Chemistry C*, 2013, **117**, 23386-23392.

[27] J, Zhang. C, Wen. L, Chen. *Journal of Physical Chemistry C*, 2018, **122**, 23829-23835.
[28] E, Farajpour. B, Sohrabi. J, Beheshtian. *Physical Chemistry Chemical Physics*, 2016, **18**, 7293-7299.
[29] B, Zhang. Z, Yuan. D, Wang. *Surfaces and Interfaces*, 2023, **41**, 103168.
[30] S, Khan. M, Yar. N, Kosar. *Computational and Theoretical Chemistry*, 2020, **1192**, 113043.
[31] S. A, Siadati. E, Vessally. A, Hosseinian. *Synthetic Metals*, 2016, **220**, 606-611.
[32] L, Safari. E, Vessally. A, Bekhradnia. *Thin Solid Films*, 2017, **623**, 157-163.
[33] U, Nosheen. A. W, Abd Jalil. S. Z, Ilyas. *Journal of Computational Electronics*, 2022, **22**, 116-127.
[34] V, Haziri. A, Berisha. M, Haliti. *Journal of Molecular Liquids*, 2024, **407**, 125176.
[35] S, Chen. S, Chen. W, Cai. *New Journal of Physics*, 2010, **12**, 125011.
[36] H, Ma. L, Ma. L. C, Ma. *International Journal of Modern Physics B*, 2019, **33(16)**, 1950166.
[37] M, Hamze. *Materials Science*, 2011, **56(8)**, 373-376.
[38] R. A, Esquivel. C, Acosta. J. A, Mendez-Gamboa. *Advances in Condensed Matter Physics*, 2015, **2015**, 1-9.
[39] B, Peles-Lemli. D, Kánnár. J. C, Nie. *Journal of Physical Chemistry C*, 2013, **117(41)**, 21509-21515.
[40] R, Alvand. M, Rezaei-Sameti. *Adsorption*, 2021, **27**, 91-104.
[41] M, Rezaei-Sameti. H, Khani. *Physical Chemistry Research*, 2022, **10(1)**, 89-104.
[42] G, Mehraein. M, Rezaei-Sameti. E, Asgary. *Journal of Molecular Structure*, 2022, **1248**, 131478.
[43] M, Rezaei-Sameti. A, Rajabi. *Chemical Papers*, 2023, **7**, 277-294.
[44] M, Rezaei-Sameti. Z, Iraji Borojeni. *Journal of Biomolecular Structure and Dynamics*, 2023, **41**, 5882-5893.
[45] H, Darougari. M, Rezaei-Sameti. *Asian Journal of Nanoscience and Materials*, 2022, **5**, 196-210.
[46] M, Rezaei-Sameti. H, Torabi. *Journal of Computational Biophysics and Chemistry*, 2023, **22**, 1-18.
[47] M, Rezaei-Sameti. A, Rezaei. *Structural Chemistry*, 2023, **53**, 1120.
[48] M. L, Laury. A. K, Wilson. *Journal of Chemical Theory and Computation*, 2013, **9**, 3939-3946.
[49] T, Yanai. D. P, Tew. N. C, Handy. *Chemical Physics Letters*, 2004, **393(1-3)**, 51-57.
[50] Gaussian Inc. *GaussView*, 2000-2003.
[51] M. J, Frisch. *Gaussian 09*, 2009.
[52] P. K, Chattaraj. A, Poddar. *Journal of Physical Chemistry A*, 1999, **103**, 8691-8699.
[53] T, Koopmans. *Physica*, 1933, **1**, 104-113.
[54] A, Savin. *Journal of Molecular Structure*, 2005, **727**, 127-131.
[55] R. F. W, Bader. *Oxford University Press*, 1990.
[56] E. R, Johnson. S, Keinan. P, Mori-Sanchez. *Journal of the American Chemical Society*, 2010, **132**, 6498-6506.
[57] D. R, Cooper. B, D'Anjou. N, Ghattamaneni. *ISRN Condensed Matter Physics*, 2012, **1**, 56.
[58] T, Koopmans. *Physica*, 1934, **1**, 104-113.
[59] R. G, Parr. R. G, Pearson. *Journal of the American Chemical Society*, 1983, **105**, 7512-7516.
[60] K. D, Sen. *Chemical Physics Letters*, 1991, **184**, 318-320.
[61] T. C, Gregory. C. D, Reed. L. K, David. *Journal of Photochemistry and Photobiology A: Chemistry*, 2023, **437**, 114484.
[62] M, Cossi. V, Barone. *Journal of Chemical Physics*, 2001, **115**, 4708-4717.
[63] R. F. W, Bader. *Journal of Physical Chemistry A*, 1998, **102**, 7314-7323.
[64] R. F. W, Bader. *Canadian Journal of Chemistry*, 1998, **76**, 973-988.
[65] S, Arulmozhi. J, Madhavan. *Materials Science and Engineering*, 2015, **73**, 012035.
[66] A. D, Becke. K. E, Edgecombe. *Journal of Chemical Physics*, 1990, **92(9)**, 5397-5403.
[67] A, Savin. O, Jepsen. J, Flad. *Angewandte Chemie International Edition*, 1992, **31(2)**, 187-188.
[68] E. R, Johnson. S, Keinan. P, Mori-Sanchez. *Journal of the American Chemical Society*, 2010, **132**, 6498-6506.
[69] L, Liu. L, Miao. L, Li. *Journal of Physical Chemistry*